Research Square

Preprints are preliminary reports that have not undergone peer review.
They should not be considered conclusive, used to inform clinical practice,
or referenced by the media as validated information.

Length Scale Dependence of the Anomalous Atomic Motion in Metallic Glasses

JIE SHEN

jie.shen@neel.cnrs.fr

1.Institute of Neel, 2.ESRF https://orcid.org/0000-0002-3432-8341

Research Article

Keywords: XPCS, relaxation dynamics, glasses

Posted Date: July 15th, 2025

DOI: https://doi.org/10.21203/rs.3.rs-7114646/v1

License: This work is licensed under a Creative Commons Attribution 4.0 International License.
Read Full License

Additional Declarations: The authors declare no competing interests.

Length Scale Dependence of the Anomalous Atomic Motion in Metallic Glasses

Jie Shen[1,2*], Fan Yang[3], Antoine Cornet[1,2], Eloi Pineda[4], Kirsten Martens[5], Yuriy Chushkin[2], Federico Zontone[2], Irene Festi[1,] Alberto Ronca[1], Nico Neuber[6], Maximilian Frey[6], Ralf Busch[6], Marco Cammarata[2], Marco di Michiel[2], Gavin Vaughan[2], Michael Sprung[7] and Beatrice Ruta[1,2*]

[1] *Institut Néel, Université Grenoble Alpes and Centre National de la Recherche Scientifique, 25 rue des Martyrs - BP 166, 38042, Grenoble cedex 9 France*

[2] *European Synchrotron Radiation Facility, 71 avenue des Martyrs, CS 40220, Grenoble 38043, France*

[3] *Institut für Materialphysik im Weltraum, Deutsches Zentrum für Luft- und Raumfahrt (DLR), 51170 Köln, Germany*

[4] *Department of physics, Institute of Energy Technologies, Center for Research in Multiscale Science and Engineering, Universitat Politècnica de Catalunya - BarcelonaTech, 08019 Barcelona, Spain*

[5] *Université Grenoble Alpes, CNRS, LIPhy, 38000 Grenoble, France*

[6] *Chair of Metallic Materials, Saarland University, Campus C6.3, 66123 Saarbrücken, Germany*

[7] *Deutsches Elektronen-Synchrotron DESY, Notkestraße 85, D-22607 Hamburg, Germany*

*Corresponding authors
beatrice.ruta@neel.cnrs.fr
jie.shen@neel.cnrs.fr

Abstract

Establishing microscopic structure–dynamics relations in glasses is essential for developing a comprehensive theory, yet remains challenging due to limited access to the relevant time and length scales. By probing density fluctuations in metallic glasses (MGs) across six decades in time and over both mesoscopic and atomic length scales, we reveal a hierarchical organization of the dynamics and provide a comprehensive framework of their anomalous compressed relaxation universally observed at the atomic level. We demonstrate that this faster-than-exponential motion emerges only at wavelengths comparable to the cluster size, and originates from internal stresses frozen during a transition from liquid-like to hyper-diffusive dynamics across the glass transition. At mesoscopic scales, stress effects vanish, and the dynamics become stationary and heterogeneous, with stretched exponential relaxations reflecting the statistically-averaged motions of rigid domains. We also identify a second independent relaxation, associated to persistent liquid-like motions, whose strength increases at large wavelength. These findings reveal the cooperative, multiscale nature of relaxations in glasses.

Main Text

Unveiling the atomic dynamics in glass former systems remains a long-standing challenge in condensed matter physics [1,2]. Its knowledge is essential for developing a microscopic theory for glasses and has broad interdisciplinary implications for understanding other complex systems. A key observable in this context is the intermediate scattering function (ISF), $f(q,t)$, which describes the temporal evolution of density fluctuations at a probed wavevector, q. This quantity can be accessed through scattering techniques using laser light [3], neutrons [4] and X-rays [5]. As the glass transition temperature, T_g, is approached from the supercooled liquid, the ISF splits in two main processes: (i) a fast decay, associated with the rattling of particles within the cages formed by neighboring atoms, and (ii) the primary α-relaxation, corresponding to cage escape and structural rearrangement [6]. While the first process occurs on picosecond timescales and is only weakly temperature dependent, the α-relaxation slows dramatically upon cooling from the melt by more than ten orders of magnitude, reaching relaxation times of hundreds of seconds near T_g.

Although the dynamics of supercooled liquids has been extensively studied [7-13], the presence of physical aging and slow relaxation processes has significantly hindered studies in the glassy state. Such investigations have only become feasible over the past decade, owing to advances

in the X-ray Photon Correlation Spectroscopy (XPCS) technique [14]. Studies in metallic glasses (MGs) have revealed a surprising dynamical crossover at T_g, where the long-time decay of the ISFs evolves from the stretched exponential form - typically associated to dynamical heterogeneities in the supercooled liquid [15] - toward an anomalous faster-than-exponential (compressed) decay in the glass [16-20]. This observation, while contrasting with some theoretical predictions [21], can be partly explained by stress-relaxation models [22-25]. Notably, similar stress-driven dynamics are observed in several soft systems, including colloids, foams, biopolymers and microgels [26-30], often marked by a transition from diffusive dynamics - described by a sub-quadratic dependence of the relaxation time, $\tau(q) \propto 1/q^2$ - to a super diffusive, ballistic-like particle motion with $\tau(q) \propto 1/q$. This behaviour has been qualitatively described by stress-relaxation models, in which dynamics are driven by random collapses of the structure in regions of high internal stress [31-33]. Whether such mechanisms apply to MGs remains an open question. Due to limitations in scattering intensity and accessible length scales, previous studies primarily focused on ISFs measured at a fixed q value, corresponding to the first sharp diffraction peak (FSDP) of the static structure factor, $S(q)$, thus precluding deeper insight into this anomalous behavior.

The advent of 4th generation synchrotrons has substantially extended the dynamical range accessible via XPCS [34]. Experiments on a $Pt_{42.5}Cu_{27}Ni_{9.5}P_{21}$ MG under high pressure have reported the emergence of hyper-diffusive motion in correspondence of the FSDP [35], which contrasts with the characteristic de Gennes narrowing observed in supercooled metallic liquids [11,12]. Temperature-scanning investigations have further shown that the compressed decay of the ISFs arises from an additional relaxation process that emerges during vitrification, specifically as the primary α-relaxation freezes out [36]. Yet, the length-scale dependence of the dynamics over a broader q-range has not been explored, and the physical origin of the compressed decay of the ISFs remains still unclear.

Here, we address this topic by presenting a detailed XPCS investigation of the ISFs in a $Zr_{46.8}Ti_{8.2}Cu_{7.5}Ni_{10}Be_{27.5}$ (Vit4) MG, spanning six decades in time and covering both mesoscopic and atomic length scales, probing the dynamics from q=0.75 Å^{-1} up to the FSDP maximum, q_{max}=2.63 Å^{-1} (**Fig. 1a)**. At the FSDP, the ISFs reflect the dynamics of the structural units defining the medium range order (MRO) [16,20], as the maximum of the FSDP is responsible for the structural periodicity in the pair distribution functions (PDF), $G(r)$, (**Fig. 1b**) [37]. In contrast, the lowest q-value provides insights into structural correlations beyond nearest-neighbor or cluster-level connections as it corresponds to spatial scales larger than the

structural correlation length, ξ [38-40]. This latter parameter defines the spatial extent of atomic order in MGs and is extracted from the exponential decay of the peak heights in the $G(r)$, using the form $f(r) = A \cdot \exp(-r/\xi)$ (**Fig. 1b**). The results are supported by additional measurements on Vit4, $Pt_{42.5}Cu_{27}Ni_{9.5}P_{21}$ and $Pd_{42.5}Cu_{27}Ni_{9.5}P_{21}$ MGs performed in another synchrotron facility (see Supplementary Information and Methods). Our data reveal a continuous transition between distinct mechanisms of collective motion approaching length scales beyond the medium range order and provide a new framework for the interpretation of the compressed decay of the ISFs in glassy systems, whose origin is a long-standing open question [14,22-25,31-33].

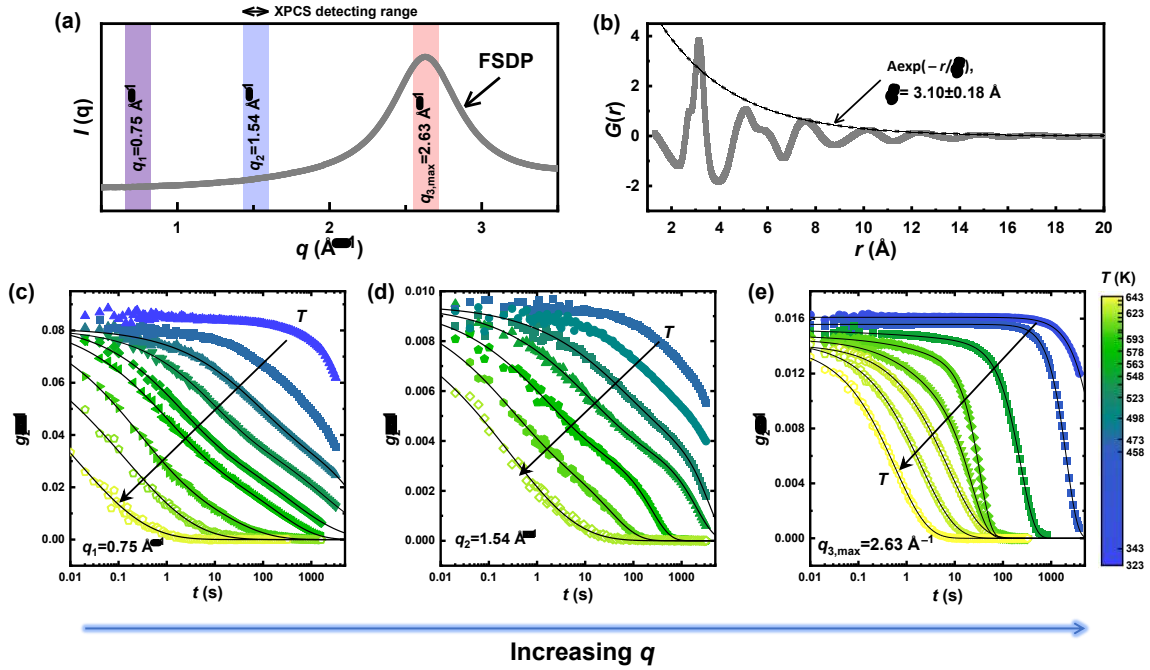


Fig. 1. Length scale dependence of the dynamics. (a) Portion of the static structure factor $S(q)$ showing the q regions where XPCS measurements have been performed, and **(b)** corresponding pair distribution functions $G(r)$ measured with synchrotron XRD at T=298 K (see Method). The black dashed line in (**b**) represents the fit of the peak heights and positions using an exponential decay function, $G(r)$=Aexp(−r/ξ). **(c)-(e)** Selection of intensity autocorrelation functions measured with XPCS at q_1=0.75 Å^{-1} **(c)**, q_2=1.54 Å^{-1} **(d)** and $q_{3,max}$=2.63 Å^{-1} **(e)**. The data have been modelled with the sum of two KWW components in the sub-T_g region and with a single KWW function in the low temperature glass and in the supercooled liquid (T_g = 613 K, determined by calorimetry).

Figure 1c-1e show intensity-intensity correlation functions, $g_2(q,t)$, measured at three characteristic q-values corresponding to distinct regions of the $S(q)$, as highlighted in **Fig. 1a**. These functions are related to the ISFs via $g_2(q,t)=1+\gamma f(q,t)^2$, where γ is the geometrical contrast arising from the partial coherence of the X-rays [5]. At each q, the dynamics was investigated during isotherms upon heating from the glass to the supercooled liquid (T_g = 613 K). Prior to each data-set, the sample was cooled from the supercooled liquid at 10 K/min to ensure identical initial states. Variation in contrasts of the $g_2(q,t)$ at the different qs come from the use of different X-ray energies (see Methods).

A clear trend emerges in the ISFs. At q_{max} the long-time decay is highly compressed at low temperatures and evolves into a stretched form in the supercooled liquid – a hallmark of the dynamical crossover in MGs at T_g [14] (see also **Fig. S1**). Additionally, a gradual increase in the amplitude of the ISFs at short times (≤10 s) signals the onset of the α-relaxation on approaching T_g, as recently observed in another composition [36]. At lower q-values, the data reveal a striking two-step decay of the ISFs which merges into a single process above T_g. Moreover, the long-time decorrelation of the ISFs becomes visibly stretched at q=0.75 Å^{-1}.

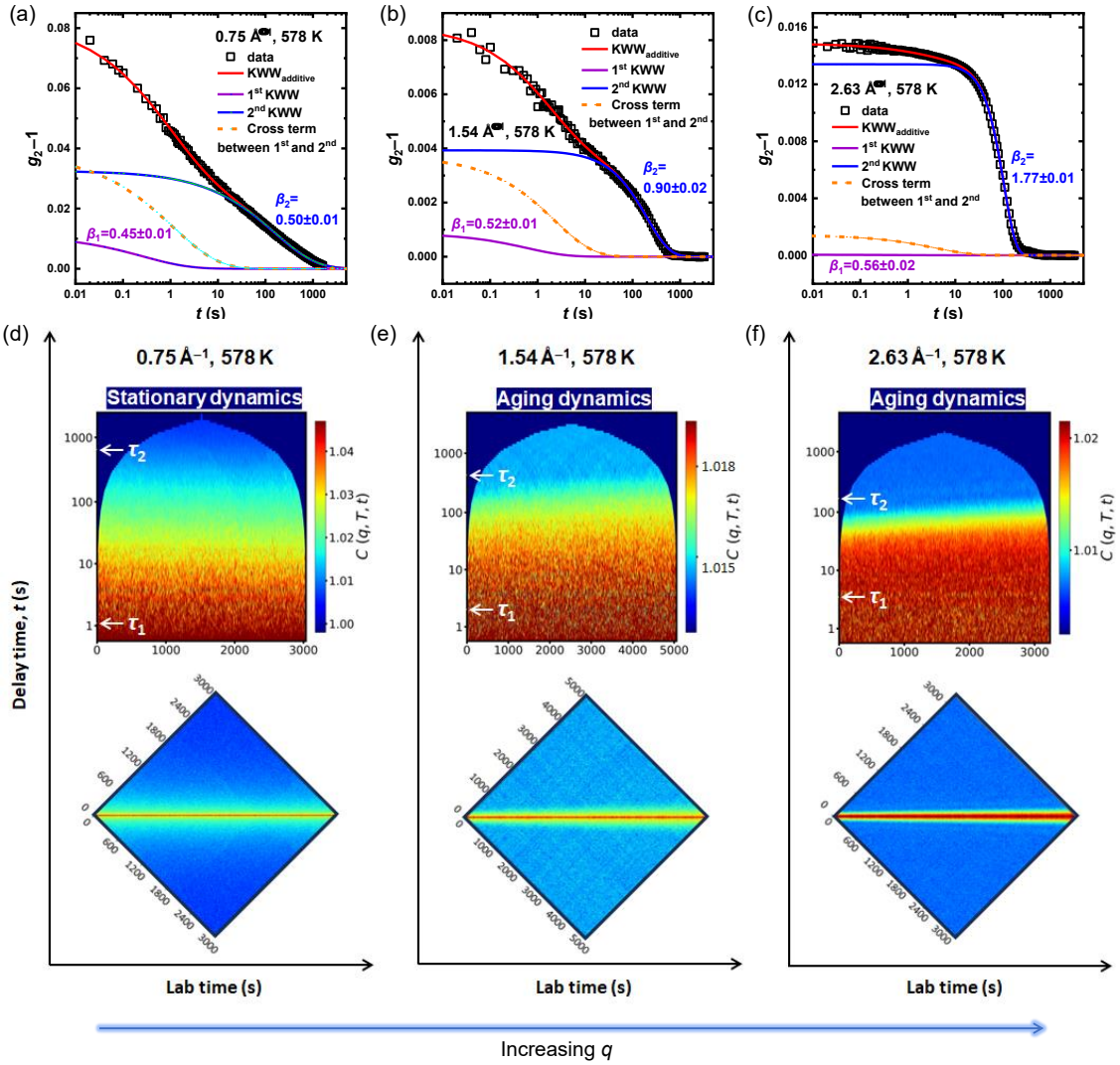


Fig. 2. Modelling of the double decay of the ISFs and temporal evolution of the dynamics. **(a)** $g_2(q,t)$ functions measured at 578 K and q=0.75 Å^{-1} **(a)**, q=1.54 Å^{-1} **(b)** and q_{max}=2.63 Å^{-1} **(c)** together with the best fits curves (red lines) with the additive model $g_2(q,t)_{add}= 1+\gamma[f_1(q,t)+ f_2(q,t)]^2$. The fitting components corresponding to the first and second decay processes are represented by solid purple and blue lines, respectively, with their associated shape factors (β) displayed accordingly, while the dashed lines correspond to the cross term. **(d)-(f)** Corresponding two times correlation functions showing stationary dynamics at q=0.75 Å^{-1} and aging at q=1.54 Å^{-1} and q_{max}=2.63 Å^{-1}(see also **Figs. S3** for results at other temperatures). The x-axis shows experimental time; the y-axis represents the delay time: the bottom panel uses linear time scaling, while the top panel employs logarithmic time binning with positions of τ_1 and τ_2 marked.

We modelled the $g_2(q,t)$ measured above T_g using the Kohlrausch-Williams-Watt (KWW) expression $g_2(q,t)=1+\gamma f_q^2\exp(-2(t/\tau)^{\beta})$, where τ is the relaxation time, f_q is the non-ergodicity

factor, and β is the shape parameter [5]. The same model describes also the low temperature data at q_{max} (**Fig. S1**), while all the curves measured between T=500 K and T_g require the use of the sum of two KWW functions $g_2(q,t)_{add}= 1+\gamma[f_1(q,t)+ f_2(q,t)]^2= 1+\gamma\left[a\exp\left(-\left(\frac{t}{\tau_1}\right)^{\beta_1}\right)+(1-a)\exp\left(-\left(\frac{t}{\tau_2}\right)^{\beta_2}\right)\right]^2$, with $0<a<1$ (black lines in **Fig. 1c-1e**) [30,41,42]. The individual components are shown in **Fig. 2a-2c** for clarity. A striking length-scale evolution is visible in the slower process: the shape parameter β_2 decreases significantly across the q-range, from a highly compressed value β_2=1.77±0.01 at q_{max} as in [43], to a strongly stretched value β_2=0.50±0.01 at q=0.75 Å^{-1}, well below the FSDP. In contrast, the faster process is consistently described by a stretched exponent $\beta_1\approx$0.5 at all q-values, with its amplitude decreasing as q increases, reaching a minimum at q_{max}. Consistent with earlier studies [36], the $g_2(q,t)$ at the FSDP can also be described by a multiplicative model; however, this approach fails at lower qs (see **Fig. S2**).

The temporal evolution of the dynamics during the isotherms is shown in **Fig. 2d-2f** using two times correlation functions (TTCFs) obtained from the instantaneous correlation of successive configurations [5]. At q_{max} and q=1.54 Å^{-1}, the TTCFs display signs of physical aging, as evidenced by the progressive broadening of the reddish intensity profile along the main diagonal over time [14]. In striking contrast, at the lowest q the dynamics remains stationary (see also **Fig. S3** for additional TTCFs). This indicates that aging occurs only when the long-time decay of ISFs is compressed, while the stretched ISFs observed at q=0.75 Å^{-1} correspond to stationary dynamics.

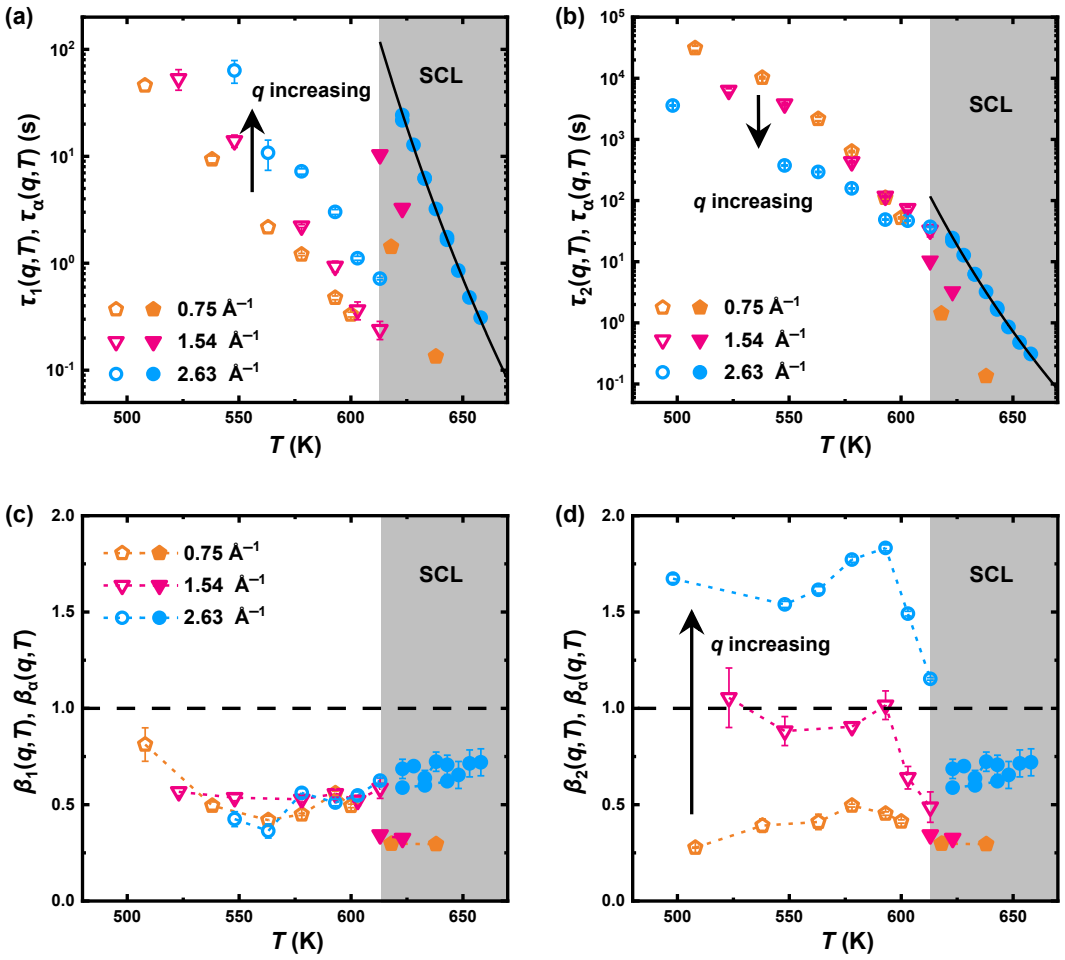


Fig. 3. Temperature and *q*-dependence of the relaxation times and KWW exponents of the two processes. Temperature dependence of the relaxation times $\tau_1(q,T)$ **(a)** and $\tau_2(q,T)$ **(b)** and of the KWW exponents $\beta_1(q,T)$ **(c)** and $\beta_2(q,T)$ **(d)** of the first (left column) and second (right column) relaxation processes. In all figures, the grey regions mark the supercooled liquid phase where the data have been described with a single KWW model function ($\tau_\alpha(q,T)$ and $\beta_\alpha(q,T)$ values in the figures). The black full lines in (**a**) and (**b**) corresponds to the Vogel-Fulcher-Tammann (VFT) equation with $\tau_\alpha(q,T) = \tau_0{*}\exp[(D{*}T_0)/(T-T_0)]$, with fitting parameters of D^*=18.8±0.2 and T_0=398±2 K, describing the evolution of the dynamics in the supercooled liquid. The arrows indicate the wavevector evolution of the parameters on approaching the FSDP from low *q*s.

The relaxation times $\tau_{1,2}(q,T)$ and $\beta_{1,2}(q,T)$ KWW exponents obtained from the data fits are shown in **Fig. 3** for various temperatures and *q*-values. The data of the supercooled liquid can be modelled with a single KWW function ($\tau_\alpha(q,T)$ and $\beta_\alpha(q,T)$).

Above T_g, XPCS probes the α-relaxation, and the ISFs display the expected temperature and q-dependence of supercooled metallic liquids [11,12,43]. At q_{max}, $\tau_\alpha(q_{max},T)$ follows the Vogel-Fulcher-Tammann (VFT) relation (**Fig. 3a, 3b**) with similar trends at the other q-values, albeit with fewer data. Furthermore, the relaxation times at q=0.75 Å^{-1}and q=1.54 Å^{-1} are smaller than at q_{max}, reflecting the de Gennes narrowing due to structure influence on liquid dynamics [37] (see **Fig. S4** for the full q-dependence in the supercooled liquid). As in other metallic glass-formers, $\beta_\alpha(q,T)$ remains stretched across all qs and decreases with increasing length scale, indicating enhanced dynamic heterogeneities at the intra-clusters level [11,12].

Below T_g, $\tau_1(q,T)$ remarkably retains the same q-dependence as the α-relaxation in the supercooled liquid but shows a weaker temperature dependence (**Fig. 3a**). Additionally, β_1 is nearly constant and close to equilibrium values at q_{max} (**Fig. 3c**). In contrast, the slow relaxation process exhibits a more complex dependence on both q and temperature: unlike the fast process, $\tau_2(q,T)$ decreases with increasing q on approaching the FSDP maximum (**Fig. 2d-2f, 3b**). Additionally, the temperature dependence is stronger at low q. The differing temperature evolutions of $\tau_2(q,T)$ in the glass and $\tau_\alpha(q,T)$ in the supercooled liquid results in a crossover near T_g where data-sets measured at different q-values intersect. Independent measurements confirm this crossover, showing that $\tau_2(q,T)$ evolves from a liquid-like q-dependence near T_g, to a hyper-diffusive regime, $\tau_2(q,T)\sim 1/q^{n(T)}$, deep in the glass (**Fig. S5**). Simultaneously, $\beta_2(q,T)$ evolves from compressed at q_{max} to stretched at the low q and depends on temperature only at q=1.54 Å^{-1} and q_{max}, where the compressed $\beta_2(q,T)$ decreases with increasing temperature towards values typical of supercooled liquids (**Fig. 3d**). A different behaviour is observed at q = 0.75 Å^{-1}, where $\beta_2(q,T)$ always maintains a constant value of ~0.4. These findings indicate that the stress-driven relaxation - manifested by compressed ISFs in MGs - is most pronounced at low temperatures and length scales comparable with the structural influence as manifested by the FSDP, while it vanishes at the mesoscopic scale where the *S(q)* is flat (**Fig. 1a**) and with increased thermal fluctuations.

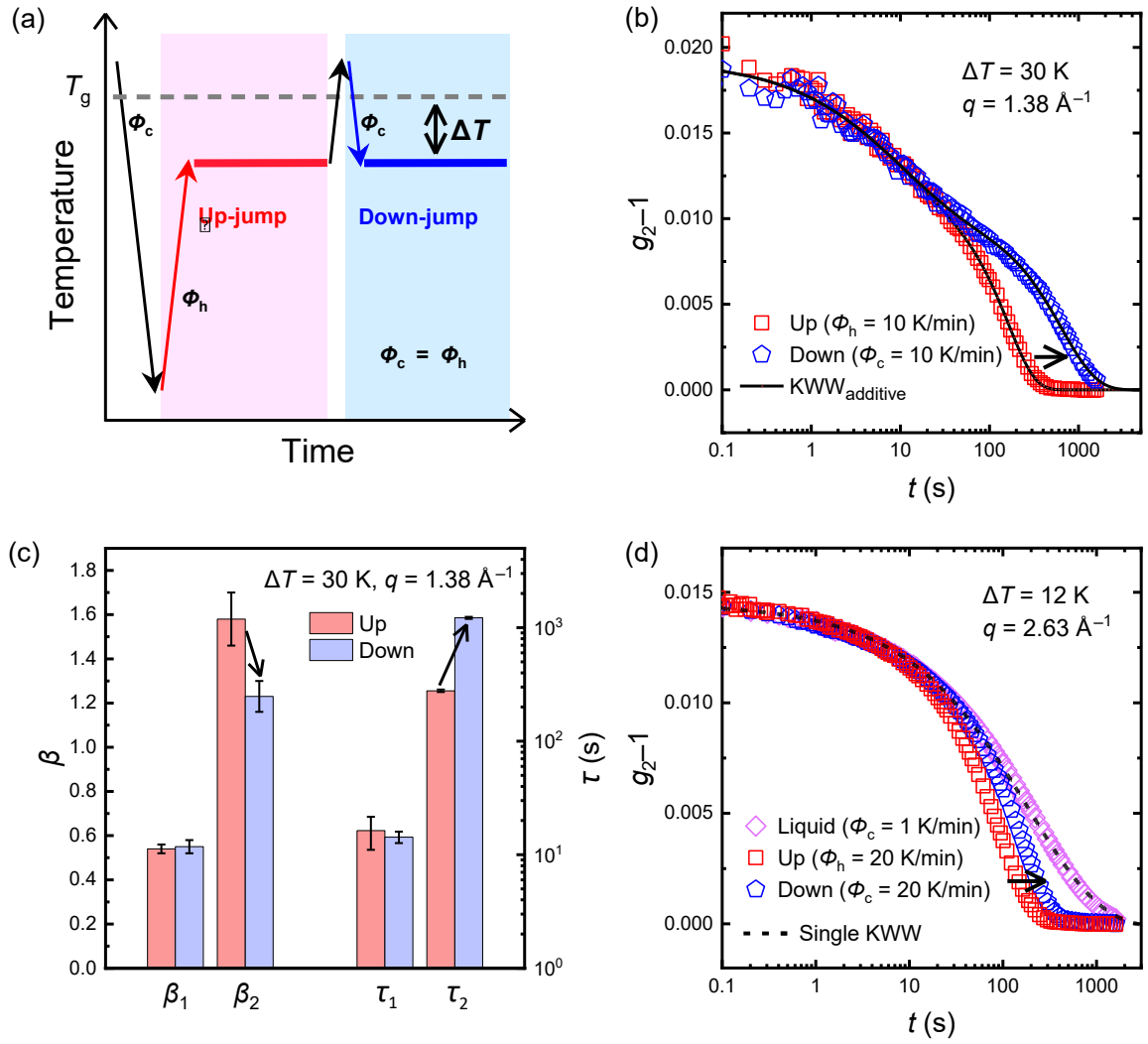


Fig. 4. Stress dependence of the fast and slow relaxation processes. (a) Sketch of the protocol used to study the effect played by thermal history on the ISFs, by comparing data measured at the same temperature T=583 K but following two different experiment path: on heating from the glass state (red line) and on cooling from the supercooled liquid phase just above T_g (blue line). Corresponding $g_2(q,t)$ functions **(b)** and fitting parameters **(c)** measured at T=583 K and q=1.38 Å^{-1} showing the influence of temperature path only on the second decay process. **(d)** $g_2(q,t)$ functions measured at T=601 K and q_{max}=2.63 Å^{-1} showing the influence of vitrification on the dynamics: squares and pentagons are measured with an up and down temperature jump to the target temperature as sketched in (**a**), while diamonds are measured in the corresponding supercooled liquid obtained by cooling at 1 K/min. The dashed line is a single KWW fitting of the liquid data. The arrows in panels **(b)**, **(c)**, and **(d)** highlight the differences in the second decay between the down-jump and up-jump measurements.

To better understand the nature of the two relaxation processes observed in the ISFs, we conducted additional experiments to examine the effect of aging, internal stresses, and vitrification kinetics. In a first test, we applied a tailored temperature protocol (**Fig. 4a**) and compared ISFs measured at the same temperature T=583 K and q=1.38 Å^{-1} but with distinct temperature paths, keeping the same heating and cooling rates to ensure the same fictive temperature, T_f, which reflects the glass thermodynamic state [44]. The selected q-value ensures a clear double decay in the ISFs, with a compressed slow component and experimentally accessible relaxation times. First, we measured the dynamics during an isotherm at T=583 K after heating the glass from room temperature (red data and parameters in **Fig. 4b** and **4c**). Then, we equilibrated the sample in the liquid and cooled it back to T=583 K (blue data and parameters). Although both glasses have the same T_f, and would thus be expected to exhibit comparable ISFs, we observe a distinct difference in the second slow relaxation process: the down-jump protocol shifts $\tau_2(q,T)$ to larger values and reduces $\beta_2(q,T)$, while the faster process remains nearly unchanged. We attribute these differences to variations in internal stresses generated during the thermal expansion and contraction: the up-jump protocol (involving continuous heating of 280 K) likely induces larger local atomic stresses compared to the milder down-jump protocol (involving continuous cooling of ~50 K). A similar evolution of $\tau_2(q,T)$ and $\beta_2(q,T)$ is also observed during physical aging, consistent with stress relaxation upon annealing (see **Fig. S6**) [17].

We now focus on the initial decay in the ISFs. To better understand the observed stationarity of this rapid relaxation, we examined the role of vitrification. Specifically, we compared isothermal measurements performed at T=601 K (12 K below the calorimetric T_g) following heating and cooling protocols at 20 K/min, both corresponding to the glassy state, with equilibrium data obtained in the supercooled liquid at the same temperature and q-value. The latter were collected by slowly cooling the high-temperature supercooled liquid at 1 K/min and performing different isothermal steps. As shown in **Fig. 4d** and in **Fig. S7** for another q-value, the fast decay observed in the non-equilibrium glass overlaps with the short-time profile of the α-relaxation measured in the supercooled liquid. This clearly indicates that the first decay in the ISFs corresponds to the unfrozen components of the α-relaxation, which still persist below T_g.

In light of these new results, the interpretation of the atomic dynamics in MGs should be revised. We attribute the first relaxation process to fast, heterogeneous motions contributing to the α-relaxation, which remain active even below T_g [36,45-48]. This interpretation is supported

by several observations: the overlap of the short-time decay of ISFs measured in both the liquid and the glass at the same temperature (**Fig. 4d** and **S6**); the liquid-like q-dependence of $\tau_1(q,T)$, reminiscent of de Gennes narrowing in equilibrium liquids (**Fig. 3a** and **S4**) [11,12]; the constant stretched $\beta_1(q,T)$ closely matching that of the supercooled phase (**Fig. 3c**) [49]; and the stationary nature of the first decay, which is unaffected by the temperature path or aging (**Fig. 4** and **S5**). Our data also reveal that the anomalous compressed decay of the ISFs universally observed in MGs occurs only at atomic scales and is accompanied by a non-trivial dependence on both q and temperature. For q-values near the FSDP, the ISFs exhibit the characteristic compressed-to-stretched dynamical crossover at T_g (**Fig. 1** and **S1**), aging (**Fig. 2** and **S3**) and a weak temperature dependence in the glassy state (**Fig. 3b**). In contrast, at the lowest q-value, the ISFs display stretched exponential decays (**Fig. 1)**, stationary dynamics (**Fig. 2**), and a strong temperature dependence (**Fig. 3b**). These observations reflect a hierarchical organization of the dynamics in MGs. Numerical studies indicate that frozen-in stress heterogeneities formed upon vitrification can still partially relax through elastically driven intermittent fluctuations, leading to faster than exponential dynamics [23,24,32,33]. The evolution of $\beta_2(q,T)$ - from compressed to stretched with decreasing q - can be understood as a statistical averaging at large length scales. While directional drift motions of rigid domains dominate at the MRO scales [20,36], these localized drifts tend to cancel statistically once the probed scale exceeds the structural correlation length of the material (**Fig.1b**), giving rise to a heterogeneous collective motion of the different domains. This interpretation aligns with recent numerical simulations of avalanche-like intermittent events in Lennard-Jones systems [20,50], where the events manifest as abrupt cluster rearrangements or micro-rotations, which tend to vanish at larger observational scales, reflecting the stabilizing effect of the statistical structural averaging over different domains. As aging is associated with stress relaxation and compressed ISFs (**Fig. S3** and **S6**), it vanishes as the probed length scale increases (**Fig. 2**), as in colloidal polycrystals under cyclic shear [51].

Thermal motion can also screen the elastic fluctuations responsible for compressed ISFs [24,33], providing a natural explanation for the dynamical crossover observed at T_g. In addition, the persistence of fast, liquid-like dynamical components below T_g – manifested in the rapid initial decay of the ISFs – implies the presence of significant mean particle displacements [47], which reduce the internal stress field associated to the formation of rigid domains. This partial activation of the α-relaxation may account for the complex behaviour of $\tau_2(q,T)$ which continuously evolves from a $\tau_2(q,T)\sim q$ dependence near T_g, to a hyper-diffusive $\tau_2(q,T)\sim 1/q^{n(T)}$

trend at lower temperatures, as $\beta_2(q,T)$ increases as well (**Fig. 3b** and **S5**). Given that the system exhibits stationary dynamics at q = 0.75 Å^{-1}, while it shows aging at higher q-values with increasingly faster rate at q_{max} (**Fig. 2d-2f**), the q-dependence of $\tau_2(q,T)$ is also expected to vary with time (**Fig. 3b**).

Compressed ISFs have been observed also in oxide and chalcogenide glasses [52-55]. In these glasses, however, the dynamics is induced by X-ray irradiation and is accompanied by structural damage. Although, no evidence of an influence of the X-rays on the dynamics and the structure was reported in MGs [52], the presence of local heating with the increased coherent flux of 4th generation synchrotrons [34] could imply some subtle contributions which would require specific investigations.

Materials and methods:

Sample preparation: Metallic glass samples with compositions of $Zr_{46.25}Ti_{8.25}Cu_{7.5}Ni_{10}Be_{27.5}$ (Vit4), $Pd_{42.5}Cu_{27}Ni_{9.5}P_{21}$, and $Pt_{42.5}Cu_{27}Ni_{9.5}P_{21}$ (all in atomic percent) were synthesized from elements with a minimum purity of 99.99%. The Vit4 alloy was melted under a high-purity argon atmosphere and subsequently processed into ribbons by melt spinning, resulting in a thickness of 30 ± 2 μm. The Pd- and Pt-based alloys were produced by pre-melting the metal elements in a Ti-gettered argon atmosphere. Elemental phosphorus was inductively alloyed with the pre-melted alloys in a fused silica tube under controlled argon. The resulting alloys were then fluxed in dehydrated high-purity B_2O_3 at 1473 K for at least 6 hours. Final MG ribbons were fabricated by melt spinning onto a rotating copper wheel under high-purity argon, obtaining samples with a thickness of 20 ± 2 μm.

XRD measurements: The atomic structure of Vit4 MG was characterized at the ID15a beamline of ESRF using a high-energy X-ray (68.5 keV) and a sample-to-detector distance of 145 mm. Scattered intensities were recorded at room temperature using a Pilatus3 X CdTe 2M detector with an exposure time of 1 minute. The resulting diffraction patterns were azimuthally integrated using standard routines from the pyFAI library. Measurements for $Pd_{42.5}Cu_{27}Ni_{9.5}P_{21}$, and $Pt_{42.5}Cu_{27}Ni_{9.5}P_{21}$ MGs were conducted at beamline P02.1 of PETRA III, DESY, using a high-energy X-ray (60 keV) with a beam size of 0.8×0.8 mm^2. The diffraction patterns were collected with a Perkin Elmer XRD1621 detector and integrated using the Fit2D software package. Further data processing was carried out with PDFgetX2 software package [56], including the calculation of structure factor, $S(q)$, and pair distribution function, $G(r)$. $S(q)$ was

obtained from the scattered intensity $I^C(q)$ as $S(q)=1+\frac{I^C(q)-|\langle f(q)\rangle|^2}{|\langle f(q)\rangle|^2}$, where $\langle f(q)\rangle=\sum_\alpha c_\alpha f_\alpha(q)$ with $f_\alpha(q)$ and c_α the atomic form factor and atomic concentration for chemical species α, respectively. $G(r)$ were then obtained through a Fourier transformation of the $S(q)$ using the relation $G(r)=\frac{2}{\pi}\int_0^{+\infty} q(S(q)\text{-}1)\sin(qr)\mathrm{d}q$.

XPCS measurements: The temperature-dependent and up/down-jump XPCS measurements were conducted at the ID10 beamline of ESRF-EBS (Grenoble, France). Due to space limitation in the experimental hutch, the maximum scattering angle accessible by XPCS at ID10 is limited to ~50 degrees. As a consequence, the energies of the X-rays has been tuned to cover the interested wave-vector range: a X-ray beam with incoming energy of 15.87 keV has been used to cover the q = 1.38 Å^{-1} – 2.63 Å^{-1}(flux ≈ 8.0×10^{11} photons/s) , with a beam size of 7.7 μm× 3.9 μm (V×H, FWHM); and a 7.67 keV incoming energy was instead employed for the low-q regime for q= 0.75 Å^{-1} – 1.7 Å^{-1} (flux ≈ 1.1×10^{12} photons/s) , with a beam size of 5.7 μm× 2.6 μm (V×H, FWHM). In both geometries, data were evaluated by considering a Δq = 0.23 Å^{-1}. Speckle patterns were recorded using an CdTe Eiger X4M detector positioned at 5.0 m from the sample, operating in continuous acquisition mode with 10 *m*s frame exposure. To ensure data consistency and eliminate aging effects, a standardized thermal protocol was implemented: prior to each measurement, the sample was cooled from the SCL state (~T_g+30 K) at a cooling rate of 10 K/min. The temperature-dependent dynamics were systematically investigated through isothermal measurements ranging from near room temperature up to the supercooled liquid phase.

The additional measurements of Vit4, and the Pd- and Pt-based MGs were conducted at beamline P10 (PETRA III) at DESY (see Supplementary Information for details). An incident energy of 8.25 keV was used, with a beam size of 1.7 μm×2.7 μm (V×H, FWHM), delivering a coherent flux of 5.0×10^{10} photons/s. The data were collected using a Si Eiger X4M detector positioned 1.8 m from the sample. Measurements were performed in the 1.41 to 2.87 Å^{-1} q-range.

For the XPCS experiments, temperature was controlled using dedicated resistively heated, water-cooled furnaces. These setups enabled operation under vacuum and achieved temperature stability better than 40 mK. At ESRF, the high coherent flux produces a local heating in the illuminated sample area [57], so temperature corrections are required when comparing data

taken at different photon energies. This effect is absent at P10 due to the lower coherent flux. To evaluate the thermal increase induced by the X-rays, we directly compared data acquired at the same q=1.54 Å^{-1} with both energies (compared to the reference condition at 15 keV, a temperature shift effect of 14 K was observed at 7.67 keV and has been corrected in the dataset).

XPCS data analysis: For each measurement, we collected series up to 500,000 speckle patterns frames for analysis. To improve the signal-to-noise ratio, time binning approach was applied prior to the computation of $g_2(q,t)$ [20]: for the full-time regime, the data were binned with 6 to 10 points per decade. The data were then processed using the sparse correlator algorithm described in reference [58] to extract the intensity-intensity correlation functions, $g_2(q,t)$. Then, the entire time was divided into 10 segments, and $g_2(q,t_a)$ was computed for each segment before being averaged. The final $g_2(q,t)$ was obtained by combining the averaged data (< 1s) with the full-time binned data. To further resolve the dynamic evolution throughout a single XPCS scan, the TTCF was computed as $C(t_1, t_2) = \langle I(t_1)I(t_2)\rangle p / (\langle I(t_1)\rangle p\langle I(t_1)\rangle p)$, where $I(t_i)$ is the intensity of a given pixel at time t_i and $\langle\cdot\rangle p$ denotes averaging over all illuminated pixels. The TTCF was derived from the correlation between scattering patterns recorded at times t_1 and t_2. In the TTCF, the diagonal ($t_1 = t_2$) reflects the short-time dynamics at each moment and corresponds to $g_2(q, t = 0)$, while horizontal and vertical traces represent $g_2(q,t)$ curves relative to specific reference times $t = |t_2-t_1|$.

Acknowledgements

We gratefully acknowledge the European Synchrotron Radiation Facility (ESRF, Grenoble, France) and Deutsches Elektronen-Synchrotron (DESY, Hamburg, Germany) for providing beamtime. The related experiments were carried out on the ID10 and ID15A beamlines at ESRF, and the P10 beamline at PETRA III (DESY). The Partnership for Soft Condensed Matter (PSCM) at the ESRF is also acknowledged for providing support facilities for sample characterization. We thank K. Lhoste for assistance on the ID10 beamline and Jean-Louis Barrat for useful discussions. This project received funding from the European Research Council (ERC) under the European Union's Horizon 2020 research and innovation program (Grant Agreement No. 948780).

Data availability statement

The data are available from the corresponding authors upon reasonable request.

Competing Interests

The authors declare that there are no financial or non-financial competing interests.

Author Contributions

JS, FY, AC, AR, EP, IF, NN, MC, YC, FZ, MS, MF, and BR carried out the XPCS experiments. JS, AC, BR, MdM, and GV were responsible for the XRD measurements. JS, FY, YC, KM and BR performed the data analysis. The manuscript was written by JS and BR, with all authors contributing to revisions. BR conceived the research idea and led the overall project.

Reference

1. Stephenson, G. B., Robert, A. & Grübel, G. Revealing the atomic dance. *Nat. Mater*. **8**, 702 (2009).
2. Berthier, L. & Reichman, D. R. Modern computational studies of the glass transition. *Nat. Rev. Phys*. **5**, 102 (2023).
3. Berne, B. J. & Pecora, R. Dynamic Light Scattering: With Applications to Chemistry, Biology, and Physics (Dover, Mineola, NY, 2000).
4. Mezei, F. Neutron Spin Echo. Lecture Notes in Physics Vol. 128 (Springer, Berlin, 1980).
5. Madsen, A., Fluerasu, A. & Ruta, B. Structural dynamics of materials probed by x-ray photon correlation spectroscopy. In Synchrotron Light Sources and Free-Electron Lasers 1–32 (Springer International, Cham, 2015).
6. Cavagna, A. Supercooled liquids for pedestrians. *Phys. Rep*. **476**, 51 (2009).
7. Ediger, M. D., Angell, C. A. & Nagel, S. R. Supercooled liquids and glasses. *J. Phys. Chem*. **100**, 13200 (1996).
8. Scalliet, C., Guiselin, B. & Berthier, L. Thirty milliseconds in the life of a supercooled liquid. *Phys. Rev. X* **12**, 041028 (2022).
9. Hecksher, T., Nielsen, A. I., Olsen, N. B. & Dyre, J. C. Little evidence for dynamic divergences in ultraviscous molecular liquids. *Nat. Phys*. **4**, 737–741 (2008).
10. Tanaka, H., Kawasaki, T., Shintani, H. & Watanabe, K. Critical-like behaviour of glass-forming liquids. *Nat. Mater*. **9**, 324–331 (2010).
11. Ruta, B. *et al.* Wave-vector dependence of the dynamics in supercooled metallic liquids. *Phys. Rev. Lett.* **125**, 055701 (2020).

12. Neuber, N. *et al.* Disentangling structural and kinetic components of the α-relaxation in supercooled metallic liquids. *Commun. Phys*. **5**, 316 (2022).
13. Handle, P. H., Rovigatti, L. & Sciortino, F. Q-independent slow dynamics in atomic and molecular systems. *Phys. Rev. Lett.* **122**, 175501 (2019).
14. Ruta, B. *et al.* Atomic-scale relaxation dynamics and aging in a metallic glass probed by x-ray photon correlation spectroscopy. *Phys. Rev. Lett.* **109**, 165701 (2012).
15. L. Berthier, G. Biroli, J.P. Bouchaud, L. Cipelletti, and W. van Saarloos, Dynamical Heterogeneities in Glasses, Colloids and Granular Media (Oxford University Press, Oxford, 2011).
16. Ruta, B., Baldi, G., Monaco, G. & Chushkin, Y. Compressed correlation functions and fast aging dynamics in metallic glasses. *J. Chem. Phys.* **138**, 054508 (2013).
17. Giordano, V. M. & Ruta, B. Unveiling the structural arrangements responsible for the atomic dynamics in metallic glasses during physical aging. *Nat. Commun.* **7**, 10344 (2015).
18. Evenson, Z., Ruta, B., Hechler, S., Stolpe, M., Pineda, E., Gallino, I. & Busch, R. X-ray photon correlation spectroscopy reveals intermittent aging dynamics in a metallic glass. *Phys. Rev. Lett.* **115**, 175701 (2015).
19. Das, A. *et al.* Stress breaks universal aging behavior in a metallic glass. *Nat. Commun.* **10**, 5006 (2019).
20. Riechers, B., Das, A., Dufresne, E., Derlet, P. M. & Maaß, R. Intermittent cluster dynamics and temporal fractional diffusion in a bulk metallic glass. *Nat. Commun.* **15**, 6595 (2024).
21. Lubchenko, V. & Wolynes, P. G. Theory of aging in structural glasses. *J. Chem. Phys.* **121**, 2852 (2004).
22. Wu, Z. W., Kob, W., Wang, W. H. & Xu, L. Stretched and compressed exponentials in the relaxation dynamics of a metallic glass-forming melt. *Nat. Commun.* **9**, 5334 (2018).
23. Ferrero, E. E., Martens, K. & Barrat, J.-L. Relaxation in yield stress systems through elastically interacting activated events. *Phys. Rev. Lett.* **113**, 248301 (2014).
24. Rodriguez-Lopez, G., Martens, K. & Ferrero, E. E. Temperature dependence of fast relaxation processes in amorphous materials. *Phys. Rev. Mater.* **7**, 105603 (2023).
25. Trachenko, K. & Zaccone, A. Slow stretched-exponential and fast compressed-exponential relaxation from local event dynamics. *J. Phys.: Condens. Matter* **33**, 315101 (2021).
26. Cipelletti, L., Ramos, L., Manley, S., Pitard, E., Weitz, D. A., Pashkovski, E. E. & Johansson, M. Universal non-diffusive slow dynamics in aging soft matter. *Faraday Discuss.* **123**, 237 (2002).

27. Cipelletti, L. *et al.* Universal aging features in the restructuring of fractal colloidal gels. *Phys. Rev. Lett.* **84**, 2275 (2000).
28. Guo, H. *et al.* Nanoparticle motion within glassy polymer melts. *Phys. Rev. Lett.* **102**, 075702 (2009).
29. Angelini, R. *et al.* Glass–glass transition during aging of a colloidal clay. *Nat. Commun.* **5**, 4049 (2014).
30. Aime, S., Truzzolillo, D., Pine, D. J., Ramos, L. & Cipelletti, L. A unified state diagram for the yielding transition of soft colloids. *Nat. Phys*. **19**, 1673–1679 (2023).
31. Bouchaud, J.-P. & Pitard, E. Anomalous dynamical light scattering in soft glassy gels. *Eur. Phys. J. E* **9**, 287 (2002).
32. Gnan, N. & Zaccarelli, E. The microscopic role of deformation in the dynamics of soft colloids. *Nat. Phys.* **15**, 683 (2019).
33. Bouzid, M., Colombo, J., Barbosa, L. V. & Del Gado, E. Elastically driven intermittent microscopic dynamics in soft solids. *Nat. Commun.* **8**, 15846 (2017).
34. Raimondi, P. *et al.* The extremely brilliant source storage ring of the European synchrotron radiation facility. *Commun. Phys.* **6**, 82 (2023).
35. Cornet, A. *et al.* Denser glasses relax faster: Enhanced atomic mobility and anomalous particle displacement under in-situ high pressure compression of metallic glasses. *Acta Mater.* **255**, 119065 (2023).
36. Frey, M. *et al.* Liquid-like versus stress-driven dynamics in a metallic glass former observed by temperature scanning x-ray photon correlation spectroscopy. *Nat. Commun.* **16**, 1 (2025).
37. Bin, W., Iwashita, T. & Egami, T. Atomic dynamics in simple liquid: de Gennes narrowing revisited. *Phys. Rev. Lett.* **120**, 135502 (2018).
38. Egami, T. & Ryu, C. W. World beyond the nearest neighbors. *J. Phys.: Condens. Matter* **35**, 174002 (2023).
39. Ma, D., Stoica, A. D. & Wang, X.-L. Power-law scaling and fractal nature of medium-range order in metallic glasses. *Nat. Mater.* **8**, 30–34 (2009).
40. Bu, H. *et al.* Accessing ultrastable glass via a bulk transformation. *Nat. Commun.* **16**, 562 (2025).
41. Jain, A. *et al.* Three-step colloidal gelation revealed by time-resolved x-ray photon correlation spectroscopy. *J. Chem. Phys.* **157**, 184901 (2022).
42. de Melo Marques, F. A. *et al.* Structural and microscopic relaxations in a colloidal glass. *Soft Matter* **11**, 466–471 (2015).

43. Amini, N., Yang, F., Pineda, E., Ruta, B., Sprung, M. & Meyer, A. Intrinsic relaxation in a supercooled ZrTiNiCuBe glass-forming liquid. *Phys. Rev. Mater.* **5**, 055601 (2021).
44. Moynihan, C. T., Easteal, A. J., De Bolt, M. A. & Tucker, J. Dependence of the fictive temperature of glass on cooling rate. *J. Am. Ceram. Soc.* **59**, 12–16 (1976).
45. Egami, T. & Ryu, C. W. Perspective: Are glasses really frozen? *J. Appl. Phys.* **137**, 074901 (2025).
46. Chang, C. *et al.* Liquid-like atoms in dense-packed solid glasses. *Nat. Mater.* **21**, 1240–1245 (2022).
47. Şopu, D., Yuan, X., Spieckermann, F. & Eckert, J. Coupling structural, chemical composition and stress fluctuations with relaxation dynamics in metallic glasses. *Acta Mater.* **275**, 120033 (2024).
48. Wang, Z., Sun, B. A., Bai, H. Y. & Wang, W. H. Evolution of hidden localized flow during glass-to-liquid transition in metallic glass. *Nat. Commun.* **5**, 5823 (2014).
49. Shang, B., Rottler, J., Guan, P. & Barrat, J.-L. Local versus global stretched mechanical response in a supercooled liquid near the glass transition. *Phys. Rev. Lett.* **122**, 105501 (2019).
50. Wang, Z. *et al.* Atomic cluster dynamics causes intermittent aging of metallic glasses. *Acta Mater.* **267**, 119730 (2024).
51. Tamborini, E., Cipelletti, L. & Ramos, L. Plasticity of a colloidal polycrystal under cyclic shear. *Phys. Rev. Lett.* **113**, 078301 (2014).
52. Ruta, B. *et al.* Hard X-rays as pump and probe of atomic motion in oxide glasses. *Sci. Rep.* **7**, 3962 (2017).
53. Alfinelli, E. *et al.* Amorphous-amorphous transformation induced in glasses by intense x-ray beams. *Phys. Rev. B* **107**, 054202 (2023).
54. Martinelli, A. *et al.* Reaching the yield point of a glass during X-ray irradiation. *Phys. Rev. X* **13**, 041031 (2023).
55. Baglioni, J. *et al.* Uniqueness of glasses prepared via x-ray induced yielding. *Rep. Prog. Phys.* **87**, 120503 (2024).
56. Qiu, X., Thompson, J. W. & Billinge, S. J. L. PDFgetX2: a GUI-driven program to obtain the pair distribution function from X-ray powder diffraction data. *J. Appl. Cryst.* **37**, 678 (2004).
57. Sun, P. *et al.* A low-background setup for in-situ X-ray total scattering combined with fast scanning calorimetry. *arXiv preprint* arXiv:2503.09183 (2025).

58. Chushkin, Y., Caronna, C. & Madsen, A. A novel event correlation scheme for x-ray photon correlation spectroscopy. *J. Appl. Crystallogr.* **45**, 807 (2012).